Karadeniz Fen Bilimleri Dergisi, 13(2), 415-433, 2023. DOI: 10.31466/kfbd.1216109

KFBD

Karadeniz Fen Bilimleri Dergisi
The Black Sea Journal of Sciences
ISSN (Online): 2564-7377 https://dergipark.org.tr/tr/pub/kfbd

Araştırma Makalesi / Research Article

A Response Surface Modeling Study on Effects of Powder Rate and Machining Parameters on Surface Quality of CoCrMo Processed by Powder Mixed Electrical Discharge Machining

Can YILDIZ[1], Faruk ÇAVDAR[2*], Erdoğan KANCA[3]

Abstract

Due to the high mechanical strength of the metals used in implant manufacture, which makes them difficult to work with using other machining techniques, electrical discharge machining (EDM) is frequently employed in the production of implants. In this study, the effect of powder ratio and other EDM parameters used in the machining of CoCrMo alloy, which used in implant production widely, with powder-mixed EDM on the surface roughness of the machined part was investigated through the response surface methodology. AISI 316L stainless steel was chosen as the electrode material, and Ti6V4Al was chosen as the additive powder, taking into account their biocompatibility properties. Using a Taguchi L_{16} array, an experimental design was created by selecting 4 levels for each parameter of additive ratio, discharge current, pulse on time (T_{on}), and pulse off time (T_{off}). The response surface method was used, along with the experimental data, to estimate how the parameters affected the arithmetic average roughness (R_a) and mean roughness depth (R_z).

Keywords: Powder Mixed EDM, CoCrMo, Response Surface Methodology, Mathematical Modeling.

Toz Oranı ve İşleme Parametrelerinin Toz Katkılı Elektro Erozyonla İşlenen CoCrMo'nin Yüzey Kalitesine Etkileri Üzerine Bir Cevap Yüzeyi Çalışması

Öz

İmplant imalatında kullanılan metallerin yüksek mekanik mukavemetleri nedeniyle diğer işleme teknikleri kullanılarak işlenmesi oldukça zor olduğundan elektro erozyonla işleme (EDM), implant üretiminde sıklıkla kullanılmaktadır. Bu çalışmada, implant üretiminde yaygın olarak kullanılan CoCrMo alaşımının toz katkılı EDM ile işlenmesinde kullanılan toz oranı ve diğer EDM parametrelerinin işlenen parçanın yüzey pürüzlülüğüne etkisi yanıt yüzey metodolojisi ile incelenmiştir. Elektrot malzemesi olarak AISI 316L paslanmaz çelik, katkı tozu olarak da biyo-uyumluluk özellikleri dikkate alınarak Ti_6V_4Al seçilmiştir. Bir Taguchi L_{16} dizisi kullanılarak, katkı oranı, deşarj akımı, ark süresi (T_{on}) ve bekleme süresi (T_{off}) parametreleri için 4'er seviye seçilerek bir deney tasarımı oluşturulmuştur. Parametrelerin aritmetik ortalama pürüzlülük (R_a) ve ortalama pürüzlülük derinliğini (R_z) nasıl etkilediğini tahmin etmek için deneysel verilerle birlikte yanıt yüzeyi yöntemi kullanılmıştır.

Anahtar Kelimeler: Toz Katkılı EDM, CoCrMo, Cevap Yüzey Yöntemi, Matematik Modelleme.

[1] Iskenderun Technical University, Institute of Graduate Studies, Hatay, Turkey, canyildiz33@gmail.com
[2] Osmaniye Korkutata University, Osmaniye Vocational School, Osmaniye, Turkey, farukcavdar@osmaniye.edu.tr
[3] Iskenderun Technical University, Faculty of Engineering and Natural Sciences, Hatay, Turkey, erdogan.kanca@iste.edu.tr

[1]https://orcid.org/0000-0001-5289-2520 [2]https://orcid.org/0000-0002-4981-6428 [3]https://orcid.org/0000-0002-7997-9631

[*]**Sorumlu Yazar/Corresponding Author** **Geliş/Received:** 08.12.2022 **Kabul/Accepted:** 28.04.2023

1. Introduction

In comparison to other non-traditional production methods, electrical discharge machining (EDM) occupies a privileged place because it uses heat energy to process electrically conductive materials, which makes it independent of the workpiece's mechanical strength and temperature resistance. Additionally, because there is no direct contact between the electrode and the workpiece, mechanical stresses, chatter, and vibration are not a concern. In the die, mold, automotive, aerospace, and surgical component industries, where parts with high mechanical strength, temperature resistance, and complex shapes are frequently used, this method is widely utilized (Cakir et al., 2013; Ho & Newman, 2003; Sharma & Singh, 2014).

Low machining efficiency and poor surface quality of conventional EDM techniques have limited further industrial uses. Due to the complicated and highly nonlinear nature of EDM, extensive studies have been conducted by numerous researchers to establish control over machining parameters and to develop new approaches to reach an ideal combination that improves machining performance. In the recent years, powder mixed electrical discharge machining has become one of the most cutting-edge and creative methods for enhancing the capabilities of EDM and removing some of its drawbacks.

A novel method termed powder-mixed electrical discharge machining (PM-EDM) solves the drawbacks of electrical discharge machining (EDM) and enhances its machining capabilities.

In this procedure, several particles, including copper, graphite, tungsten, aluminum, and chromium, are combined with the dielectric fluid. To effectively fill the spark gap with these additive particles, a specifically designed stirrer mechanism stirs the fine powder particles into the tank. The EDM process becomes more stable as a result of these electrically conductive powder particles' reduction in the dielectric fluid's insulating strength and increase in the spark gap distance between the tool electrode and workpiece. This improves the material removal rate (MRR) and surface finish of the workpiece. Surfaces created by the PM-EDM method have great resistance to corrosion and abrasion (Jawahar et al., 2019; Rajkumar & Vishwakamra, 2018; Sharma & Singh, 2014).

The use of PM-EDM in the biomedical field has recently received significant interest (ERDEM & KILIÇ, 2020; Kumar et al., 2020; Rajkumar & Vishwakamra, 2018). Along with increasing corrosion and wear resistance, PM-EDM has significantly improved the mechanical and fatigue life of orthopedic implants (Iacono et al., 2016; Ntasi et al., 2010; Prakash et al., 2015). However, there have recently been reports of using PM-EDM to deposit a nano-porous and biocompatible layer on the machined implant surface. Strong bone-implant bonding is provided by this deposition layer (Al-Amin et al., 2020).

Due to their great biocompatibility, good mechanic wear, and corrosion resistance, CoCrMo alloys are frequently employed as biomaterials for orthopedic implants, particularly in artificial hip and knee joints, as well as the infrastructure of metal-ceramic implants (Augustyn-Pieniążek et al., 2013; Fazira et al., 2013).

Numerous research on the processing of Co-Cr-Mo alloy using EDM, with or without powder additions, are available in the literature. The processing of Co-Cr-Mo material with classical EDM was examined in these studies to determine the effects of various processing parameters, electrode types, and dielectric fluids on the surface characteristics of the workpiece, biological response, corrosion resistance, in vitro hemocompatibility, electrochemical properties, and cytocompatibility of the surface. Graphite, W, Cu, Cu-W, and Ti as electrode materials were used in this research (Chakmakchi et al., 2021; Iranmanesh et al., 2017; Mahajan et al., 2019; Mahajan & Sidhu, 2019b, 2019a; Mahajan Amit and Sidhu, 2019). In some other studies, the effect of adding Fe2O3and γ-Fe2O3 nanopowder to the dielectric liquid at different rates on the material removal rate was investigated (N. Elsiti et al., 2017; N. M. Elsiti & Noordin, 2017).

In this study, the effects of powder ratio and machining parameters in the PM-EDM process on surface roughness metrics i.e. R_a and R_z, of the CoCrMo workpiece are analyzed and modeled through RSM. In the experimental PM-EDM process, 316L and Ti6V4Al were utilized as the electrode and dielectric additive respectively in the PM-EDM of Co-Cr-Mo. The fact that 316L and Ti6V4Al are currently utilized as implant materials and that there is no biocompatibility issue if residues from these materials are left on the surface of the workpiece as a result of processing were taken into consideration while selecting these materials (Abdel-Fattah et al., 2011; Sales et al., 2016; ÖPÖZ et al., 2019; Ali et al., 2019).

Four levels for the additive powder ratio, discharge current, pulse on time (T_{on}), and pulse off time (T_{off}) variables were established in the investigation, and a Taguchi L_{16} orthogonal experimental design was developed in the study. The determined parameters were applied to the constructed samples, and each sample's R_a and R_z surface roughness values were then calculated. With the use of these values, response surfaces for R_a and R_z were created and examined.

2. Materials and Methods

2.1. Experiment Design

In addition to further streamlining and standardizing the design of experiments (DOE), the Taguchi technique produced guidelines to conduct the experiments, reducing the number of factor combinations needed to assess the factor effects. L_{16} orthogonal array with 5 variables and 4 levels was used in this investigation. The independent variables (factors) are chosen to be the powder ratio (w), discharge current (I), pulse on time (T_{on}), and pulse off time (T_{off}). The dependent variables (responses), however, are R_a (the arithmetic mean height of the profile) and R_z (the maximum height of the profile). Experiment set values of the variable and corresponding experiment results is listed in Table 1.

Table 1. Experimental set values of the factors and corresponding response values

Experiment No	Powder Ratio (g/l)	Discharge Current (A)	T_{on} (µs)	T_{off} (µs)	R_a (µm)	R_z (µm)
E1	0	9	180	18	5.26	28.42
E2	0	12	240	24	6.94	34.25
E3	0	15	300	30	9.29	42.45
E4	0	18	360	36	11.98	53.94
E5	2	9	240	30	5.39	27.86
E6	2	12	180	36	6.99	35.31
E7	2	15	360	18	12.52	55.68
E8	2	18	300	24	9.78	47.09
E9	4	9	300	36	5.21	26.96
E10	4	12	360	30	8.11	37.83
E11	4	15	180	24	8.76	39.58
E12	4	18	240	18	8.30	39.20
E13	8	9	360	24	5.80	28.59
E14	8	12	300	18	8.05	37.10
E15	8	15	240	36	7.79	40.64
E16	8	18	180	30	9.42	44.60

2.2. Material and Experimental Procedure

In this study, ASTM F1537-11 grade CoCr28Mo6 alloy, with chemical composition stated in Table 2, in round bar form was used. The samples were cut in 30 mm diameter and 10 mm thickness then the surfaces were polished.

Table 2. Chemical composition of the CoCr28Mo6 bar used in the study

C	Si	Mn	P	S	Cr	Fe	Ni	Mo	N	W	Al	Co
0.051	0.74	0.77	0.005	0.0004	27.9	0.22	0.12	5.41	0.163	0.01	0.01	Balance

AISI 316L electrodes were used to process samples. During the experimental process, Petrofer Dielektrikum 358 EDM oil was used mixed with Ti6V4Al powder in different ratios as dielectric fluid.

Experiments have been conducted on the Best-3000S ZNC EDM machine. A closed loop tank equipped with a pump was designed and constructed as seen in Figure 1.

Figure 1. Closed loop tank used in the experimental processes

2.3. Surface Roughness Measurements

The mostly used roughness measurement in the manufacturing industry is R_a, which is the arithmetic average of the deviations from the mean line. On the other hand, R_a is not sufficient to give information about the depth of the peaks or valleys. To better understand the surface quality R_a may be used with R_z which is the average of the absolute deviations of the five highest peaks and the five deepest valleys from the mean line. For this reason, the effects of the powder ratio and machining parameters both on R_a and R_z are analyzed in this study (David Whitehouse, 2002).

The roughness of the machined surfaces of the samples has measured by using a Hommel Etamic C8000 profilometer equipped with a TKU300 model probe. Four measurements have been taken from each specimen. Arithmetical mean roughness value (R_a) and mean roughness depth (R_z) values are determined for each measurement and average values for each specimen are listed in Table 3.

Table 3. ANOVA table of R_a and R_z models

Response		R_a (µm)	R_z (µm)
Model Type		2FI	2FI
Model DF		7	5
Model	F *value*	14.83	14.12
	p-value	0.0005	0.0003
w	*F value*	4.93	28.39
	p-value	0.0571	0.0003
I	F *value*	5.5	4.73
	p-value	0.047	0.0547
T_{on}	F *value*	5.77	10.22
	p-value	0.0431	0.0095
T_{off}	F *value*	5.88	10.37
	p-value	0.0415	0.0092
$W*T_{on}$	F *value*	7.7	-
	p-value	0.0241	-
$W*T_{off}$	F *value*	-	8.31
	p-value	-	0.0163
$I*T_{off}$	F *value*	4.26	-
	p-value	0.073	-
$T_{on}*T_{off}$	F *value*	6.45	-
	p-value	0.0347	-
R^2		0.928	0.876
R^2_{adj}		0.866	0.814

2.4. Response Surface Methodology

Response surface methodology (RSM) is frequently used in research endeavors where multiple dependent variables are governed by many independent factors. With the use of suitable experiment designs and analyses, response surface methodology is a collection of mathematical and statistical tools for determining the extent to which independent variables (factors) impact dependent variables (responses).

The product attributes or performance values that result from a certain combination of factor values are referred to as the dependent variable or response. Independent variables or factors are variables or factors whose values can be altered by the researcher to achieve certain objectives.

If unknown relation between a response and independent parameters is stated as (x_1, x_2, …, x_k,) such as

$$y = f'(x)\,\beta + \varepsilon \tag{1}$$

where y is the response, and *f(x)* is a vector function of *x*'s ($x_1, x_2, ..., x_k,$) with q terms that include exponents up to a point and cross products between them, β is a vector related with *f(x)* containing *q* unknown constants, ε is a random experimental error with zero mean.

Utilizing experimental set values and the measurement data shown in Table 3, response surface models for R_a and R_z with a two-factor interaction were created. To acquire the best model fit scores, such as the F-value, p-value, R^2, and R^2_{adj}, response surface model degrees were calculated through trials and errors.

3. Findings and Discussion

3.1 ANOVA Results

With the use of the information in Table 2, an analysis of variance (ANOVA) has been done within the RSM's purview to determine the effects of independent variables on R_a and R_z. A succinct list of the ANOVA findings and model fit metrics like R^2 and R^2_{adj} is presented in Table 3. In the ANOVA table, the model's F-value indicates the proportion of explained to unexplained variance. If the F-values of the model and terms are higher than the critical F-value in the 95 percent confidence interval, the model is significant. The relevance of the model or phrase is additionally assessed using the p-value. If the p-value is low enough, the model or term should have a considerable impact on the result (less than 0.05 for the model and 0.1 for a term) (Dinov, 2020; Kumar et al., 2020; Mesalamy & Youssef, 2020; Myers et al., 2016).

The model's F-value indicates the ratio of explained to unexplained variance. If the F-values of the model and terms are higher than the critical F-value in the 95 percent confidence interval, the model is significant. The relevance of the model or phrase is additionally assessed using the p-value. If the p-value is low enough, the model or term should have a considerable impact on the outcome (less than 0.05 for the model and 0.1 for a term).

R_a has been the subject of a 2FI regression model with 7 degrees of freedom, which is the number of terms included in the model. The model's F-value and p-value are 14.83 and 0.0005 in Table 3, respectively, indicating that it is significant and that there is only a 0.05% possibility that the noise could cause the F-value to be this high. Table 3 shows the model's R^2 and R^2_{adj} values as 0.928 and 0.866, respectively. This indicates very good variance in the response caused by variation in the independent variables, and the model does not contain extraneous terms.

Significant terms in the regression model of *Ra* are w, I, T_{on}, T_{off}, $w*T_{on}$, $I*T_{off}$, and $T_{on}*T_{off}$. Regression coefficients of the actual and coded factors included in the R_a model are listed in Table 4.

The regression model equation was constructed by using actual factors and their coefficients are stated in Equation 2.

Table 4. Regression coefficients of R_a response model in terms of coded and actual factors.

Factors	Coefficients of coded factors	Coefficients of actual factors
Constant	8.02	-3.1197
w	-0.4029	1.383
I	0.7141	-0.281
T_{on}	0.4209	0.0671
T_{off}	-0.5003	-0.0044
w T_{on}	-0.7318	-0.0058
I T_{off}	0.2903	0.0203
T_{on} T_{off}	-0.3848	-0.0013

$$R_a = 1.383w - 0.281I + 0.0671T_{on} - 0.0044T_{off} - 0.0058wT_{on} + 0.0203IT_{off} - 0.0013T_{on}T_{off} - 3.1197 \quad (2)$$

A 2FI regression model with 5 degrees of freedom has been developed for R_z response. F-value and p-value for the R_z model are 14.12 and 0.0003, respectively, showing that it is significant and that there is only a 0.05% chance that the noise might be the reason for the high F-value. The model's R^2 and R^2_{adj} values are 0.876 and 0.814, respectively, according to Table 3. This shows that the model is free of redundant terms and that there is a very good variance in the response resulting from the change in the independent variables.

The significant terms in the regression model of R_z are *w, I*, T_{on}, T_{off}, and $w*T_{off}$. Table 5 provides the regression coefficients for the real and coded components used in the R_z model. The coefficients of the regression model equation that was created using actual factors are given in Equation 3.

Table 4 shows that R_a is favorably impacted by an increase in *I*, T_{on}, *and* $I*T_{off}$, while R_a is negatively impacted by an increase in *w*, T_{off}, $w*T_{on}$, and $T_{on}*T_{off}$. Additionally, it is implied that among the single terms, *I* and T_{off} have the most impact on R_a.

It is clear from the coefficients of coded factors in Table 5 that *w*, T_{off}, and $w*T_{off}$ have a diminishing impact on R_z, even though I and T_{on} are parameters that raise R_z. On the other hand, it is evident that *w* and T_{on}, respectively, have the greatest impact on the change in R_z.

Table 5. Regression coefficients of R_z response model in terms of coded and actual factors.

Factors	Coefficients of coded factors	Coefficients of actual factors
Constant	33.24	6.083
w	-6.07	3.441
I	2.46	0.920
T_{on}	3.89	0.073
T_{off}	-3.7	0.197
$w*T_{off}$	-2.83	-0.222

$$R_z = 3.441w + 0.920I + 0.073T_{on} + 0.197T_{off} - 0.222wT_{off} + 6.083 \quad (3)$$

3.2. Discussions

To predict their values for the points where trials were not conducted as part of the study, a regression model of R_a and R_z was developed. In order to comprehend how changes in the independent factors affect the dependent variables, 3D surface models were also developed. Two elements are held constant in each graph while the changes in the other factors are displayed because the effect of two independent variables on a response can be simultaneously visualized in three-dimensional (3D) graphics.

3.2.1 Arithmetical mean roughness (R_a)

The variation of R_a with respect to w and I for constant values of T_{on} and T_{off} is shown in Figure 2. As can be observed in Figure 2a, R_a only marginally rises with an increase in I from 9 to 18 A for constant values of T_{on} and T_{off} at 180 and 18 µs, respectively. However, given the constant I value, it grows linearly as the powder rate climbs from 0 to 8 g/l.

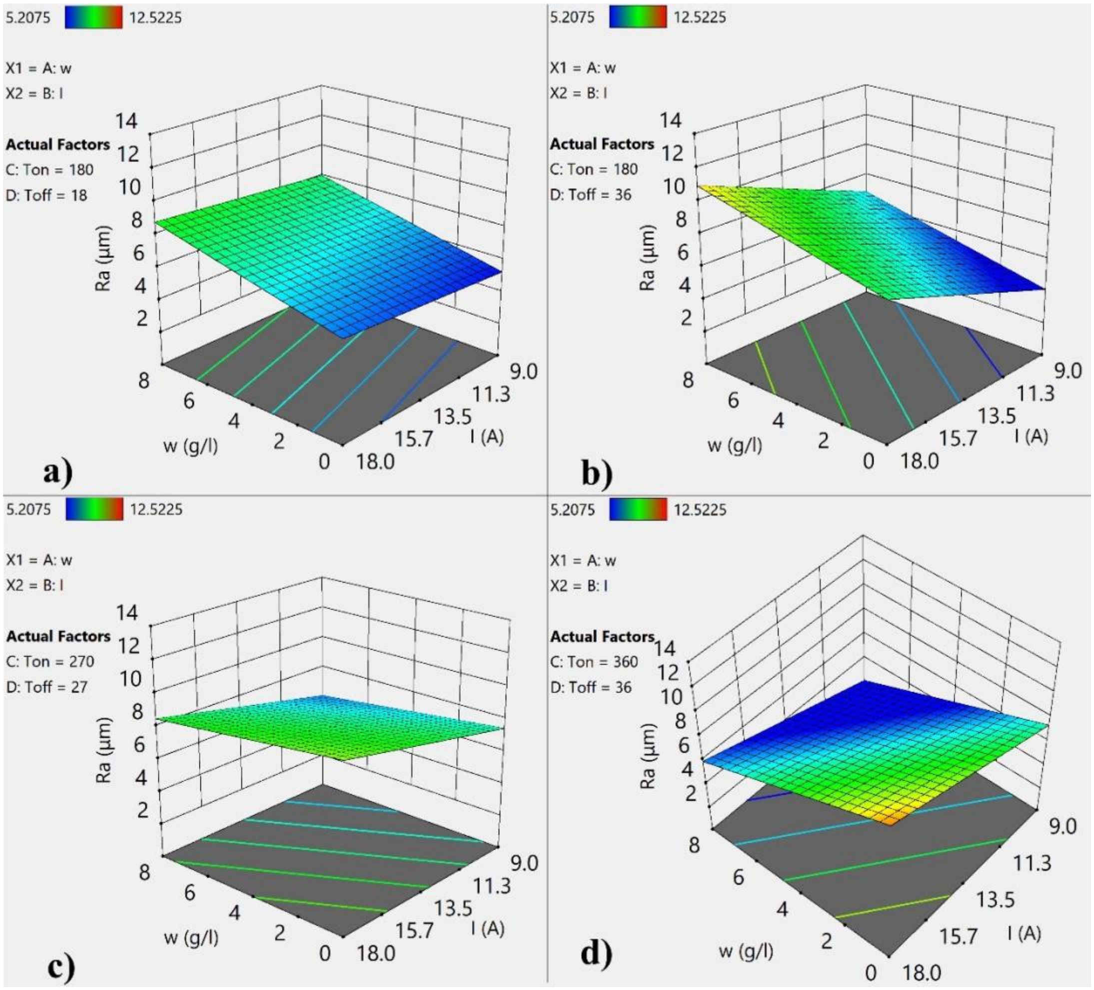

Figure 2. Change in R_a with *w* and *I* for constant values of a)T_{on}= 180, T_{off}=18 µs; b) T_{on}= 360, T_{off}= 36 µs; c)T_{on}= 270, T_{off}= 27 µs; d)T_{on}= 360, T_{off}=36 µs

In Figure 2b, it is seen that R_a increases linearly with increasing current at constant values of 180 and 36 µs for T_{on} and T_{off}, respectively. Similarly, R_a increases linearly with an increasing powder ratio.

R_a increases linearly with the increase in current in Figure 2 c, where T_{on} is 270 µs and T_{off} is 27 µs, but the slope is lower than that in Figure 2b. On the other hand, R_a decreases linearly as the powder content rises.

As observed in the constant values of T_{on} and T_{off} at 360 and 36 µs, respectively, in Figure 2d, R_a changes directly with current and inversely concerning the powder ratio Figure 2c. It is evident that the slope is higher in Figure 2d than in Figure 2c, though.

When the four plots in Figure 2 are analyzed collectively, it is concluded that when the T_{on} time interval is nearly 180 µs, the increase in the powder ratio has the impact of increasing R_a. This effect is found to diminish as the T_{on} value rises and to reverse as the T_{on} value approaches 360 µs. On the other hand, it is seen that the influence of current grows as this value increases, even though the effect of current on R_a is relatively minimal when *Toff* is 18 µs.

Figure 3's graphs illustrate how R_a varies with T_{off} and the powder ratio for constant current and T_{on} values. R_a increases with increasing powder content but decreases with increasing T_{on} at constant values of 9 A of current and 180 µs of T_{on} (Figure 3a).

Figure 3b shows that R_a decreases when the powder ratio and T_{off} value rise while the current is fixed at 9 A and Ton 360 µs.

According to (Figure 3c), for constant current and T_{on} values at 14 A and 270 µs, respectively, R_a marginally decreases with an increase in the powder ratio and T_{off}.

As demonstrated in Figure 3d, the R_a drops linearly as the powder ratio and T_{off} increase when the current is 18 µs and the T_{on} is 360 µs. The slope of the variation of R_a with related to T_{off} decreased and the slope of the variation with respect to *w* rose when this graph is compared with Figure 3b.

When the three graphs in Figure 3 are compared, it can be seen that an increase in current causes a change in R_a corresponding to an increase in powder ratio, which is positive at 9 A, neutral at 14 A, and negative at 18 A. On the other hand, it is considered that a rise in current causes a drop in R_a, just as an increase in T_{off} causes a decrease in current.

Examining the influence of T_{on} on R_a trends reveals that as T_{on} rises, R_a's correlation to the powder ratio shifts from positive to negative. Additionally, it can be noted that R_a has a greater tendency to decline with T_{off} as T_{on} grows.

Figure 4's graphs illustrate how R_a varies with T_{on} and T_{off} at constant values for the additive ratio and discharge current. Figure 4a shows that the dielectric fluid is being used without any powder and that the current value is constant at 9 A. R_a increases linearly as T_{on} increases, and its slope decreases as T_{off} increases. R_a, on the other hand, is independent of T_{off} in the region where T_{on} is 180 s µs. R_a rises with rising T_{off} for higher values of T_{on}.

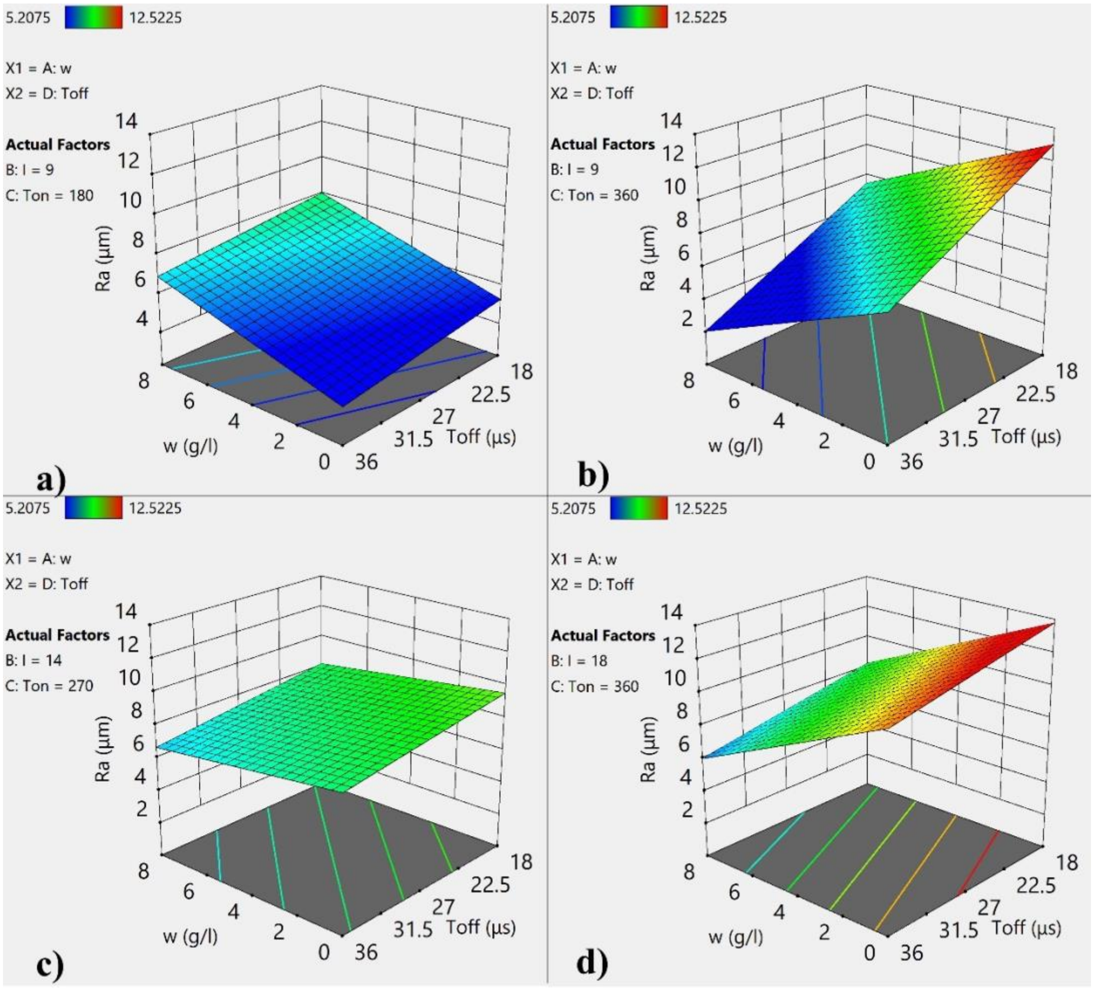

Figure 3. Change in R_a with w and T_{off} for constant values of a) I= 9 A, T_{on}= 180 µs; b) I=9 A, T_{on}= 360 µs; c) I= 14 A, T_{on}= 270 µs; d) I= 18 A, T_{on}= 360 µs

In Figure 4b, R_a falls with an increase in T_{off} when the current is increased to 18 A while doing powder-free processing; however, this scenario is reversed when the T_{on} value is raised to 360 µs. R_a is shown to rise linearly as T_{on} increases. However, as T_{off} increases from 18 µs to 36 µs, the slope of this rise becomes less steep.

When the discharge current is 14 A and the additive rate is 4 g/l (Figure 4c), it can be seen that the R_a rises as T_{on} rises in the 18 µs T_{off} region. On the other hand, R_a decreases slightly as T_{on} increases in the region where T_{off} is 36 µs. Additionally, it can be shown that R_a and T_{off} are directly proportional at low levels of T_{on} whereas R_a and T_{off} are inversely proportional at large values of T_{on}.

When the discharge current is 18 A and the additive rate is 8 g/l, it can be seen that rise in R_a with a rise in Toff in the 18 µs region of T_{on}. R_a increases as T_{off} in the region where it is 36 µs lowers with a moderate slope. Additionally, R_a nearly never changes with T_{on} in the area where T_{off} is 18 years old. R_a changes in an inverse correlation to T_{on} in the region where T_{off} is 36 µs.

When Figures 4a, 4c, and Figures 4b, 4d, are compared, it can be observed that the influence of T_{on} and T_{off} on R_a diminishes as the powder content rises. The increase in I, on the other hand, makes the impact of T_{off} on R_a more obvious, as can be seen when the four graphs in Figure 4 are analyzed collectively.

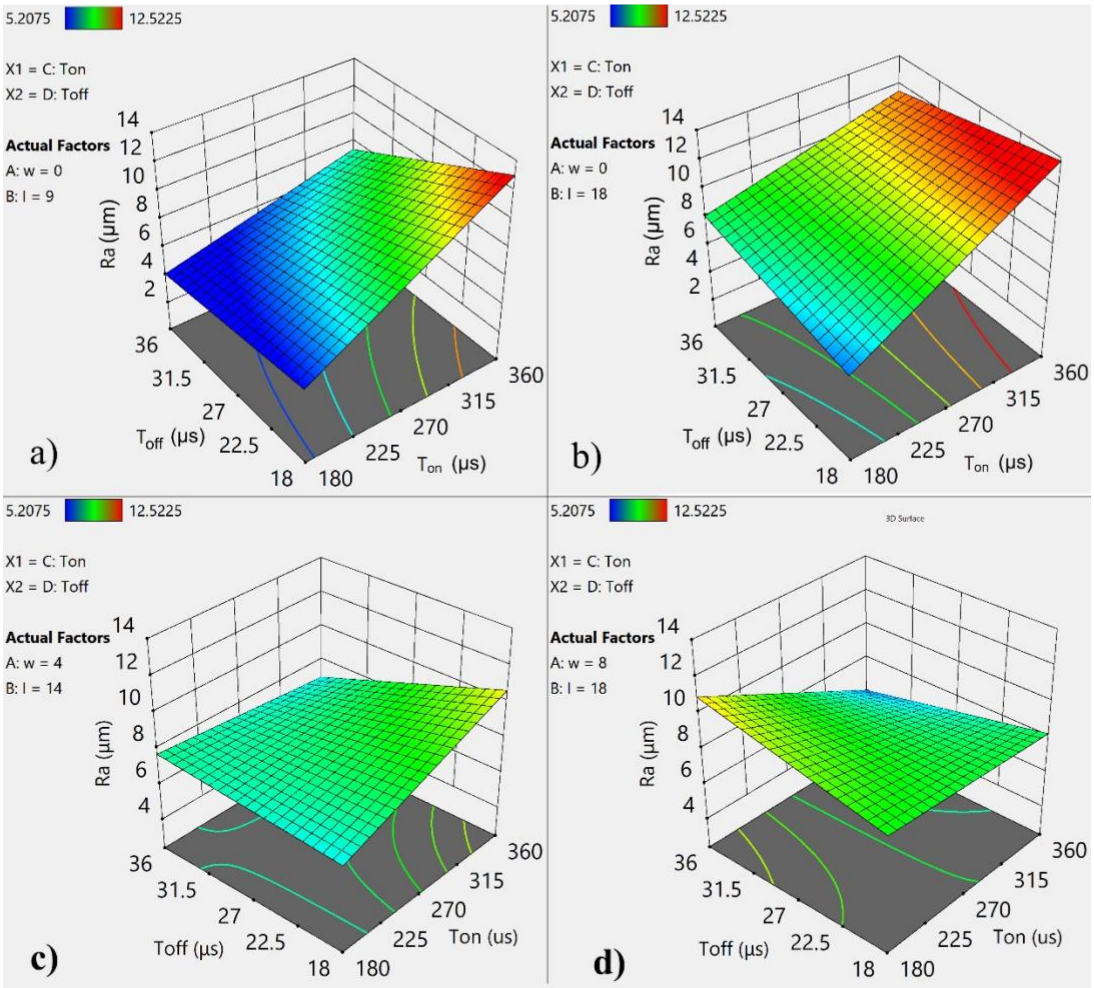

Figure 4. Change in R_a with T_{on} and T_{off} for constant values of a) w= 0, I= 9 A; b) w= 0, I= 18 A; c) w= 4 g/l, I= 14 A; d) w= 8 g/l, I= 18 A

3.2.2. Ten-point mean roughness (Rz)

Figure 5 shows the fluctuation of R_z for constant values of T_{on} and T_{off} according to the powder ratio and discharge current. Figure 5a shows that R_z essentially stays the same with the powder ratio at constant values of 180 µs and 18 µs for T_{on} and T_{off}, respectively. On the other hand, as the discharge current rises from 9 A to 18 A, R_z similarly increases linearly.

As shown in Figure 5b, R_z dramatically reduces with rising additive content when T_{on} is 180 µs and T_{off} is 36 µs, although R_z barely increases with increasing discharge current.

When Figure 5c is evaluated, it can be shown that for 270 µs T_{on} and 28 µs T_{off} values, R_z varies inversely with the powder ratio and is directly proportionate to the current.

Once more, R_z grew in direct proportion to the current at 360 µs of T_{on} and 36 µs of T_{off}. The powder ratio and R_z vary inversely, but the variance was more than in Figure 5c.

When the four graphs in Figure 5 are compared, it can be observed that an increase in T_{on} raises the R_z value for all other factor values. On the other side, as T_{off} rises, the impact of the dust ratio on R_z grows.

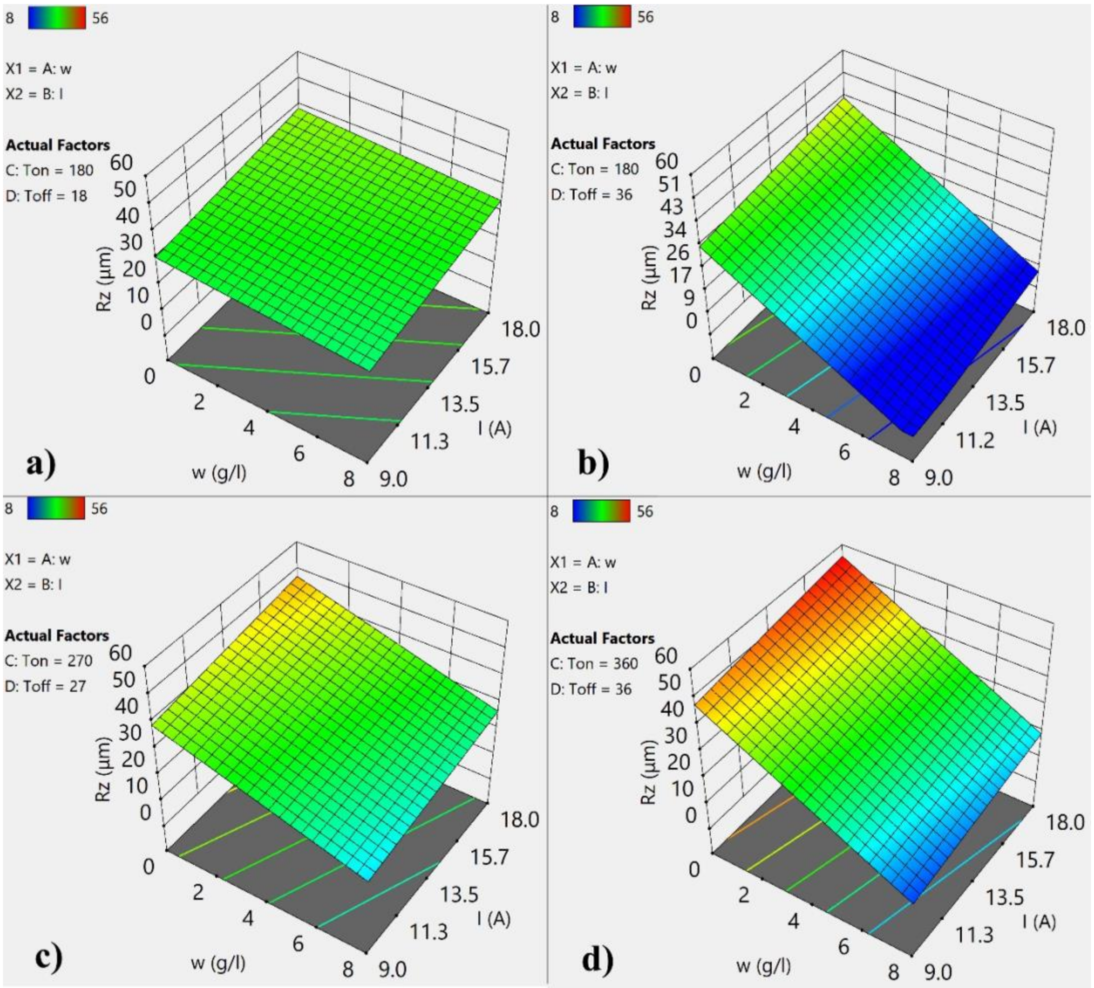

Figure 5. Change in R_z with w and I for constant values of a)T_{on}= 180, T_{off}= 18 µs; b) T_{on}= 360, T_{off}= 36 µs; c)T_{on}= 270, T_{off}= 27 µs; d)T_{on}= 360, T_{off}= 36 µs

For constant levels of discharge current and Ton, Figure 6 depicts the evolution of R_z with powder ratio and T_{off}. Figure 6a shows that while the additive ratio is close to zero, R_z almost does not change according to the current, while at high powder ratios, R_z declines linearly with the increase in T_{off}. Figure 6a was made for the constant values of the discharge current of 9 a and T_{on} for 180 µs. The slope here likewise grows as T_{off} approaches 36 µs. On the other hand, for low values of T_{off}, R_z declines with an increase in powder content and has a very tiny slope.

Examining Figures 6b and 6c reveals that the graphs created for the current values of 9 A, T_{on} 360 s, 14, and 270 are similar to Figure 6a, with the exception that R_z's maximum and minimum values are now higher. R_z takes higher values than in any other situation in figure 6d, where the present value is 16 and the T_{on} value is 36.

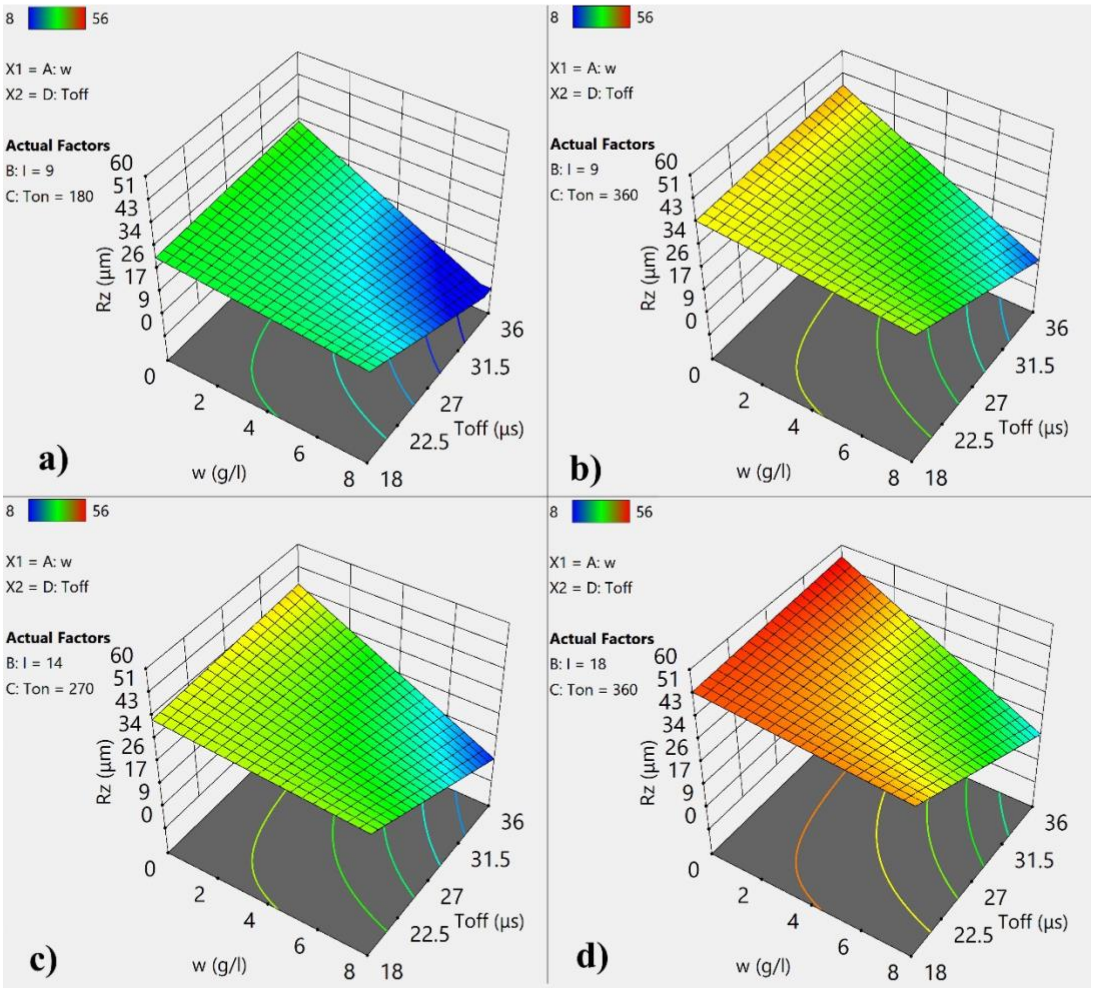

Figure 6. Change in R_z with w and T_{off} for constant values of a)T_{on}= 180, T_{off}= 18 µs; b) T_{on}= 360, T_{off}= 36 µs; c)T_{on}= 270, T_{off}= 27 µs; d)T_{on}= 360, T_{off}= 36 µs

Figure 7 shows the fluctuation of R_z based on T_{on} and T_{off} for constant additive ratio and current levels. Figures 7a and 7b were created, with figure 7a representing the fixed value of the powder rate at zero and discharge current at 9 A, respectively. R_z somewhat increased with an increase in T_{off} and slightly dropped with an increase in T_{on} in both of these graphs. The R_z values in Figure 7b are somewhat greater than those in Figure 2b, which distinguishes the two graphs.

Figure 7c was made for an additive ratio of 4 g/l and current 14 values, and Figure 7d was created for a powder ratio of 8 g/l and current 18 A. R_z increases with an increase in T_{on} in these graphs, while it decreases with an increase in T_{off}. The slope of the change with R_a, T_{off}, and T_{on} increased in Figure 7d, which makes the two graphs different from one another.

When the graphs in Figure 7 are compared, it can be inferred that for all values of the other parameters, the effect of an increase in current on R_z increases. The shift in R_z with T_{off} and T_{on} became more obvious as the additive ratio increased from 0 to 8 g/l.

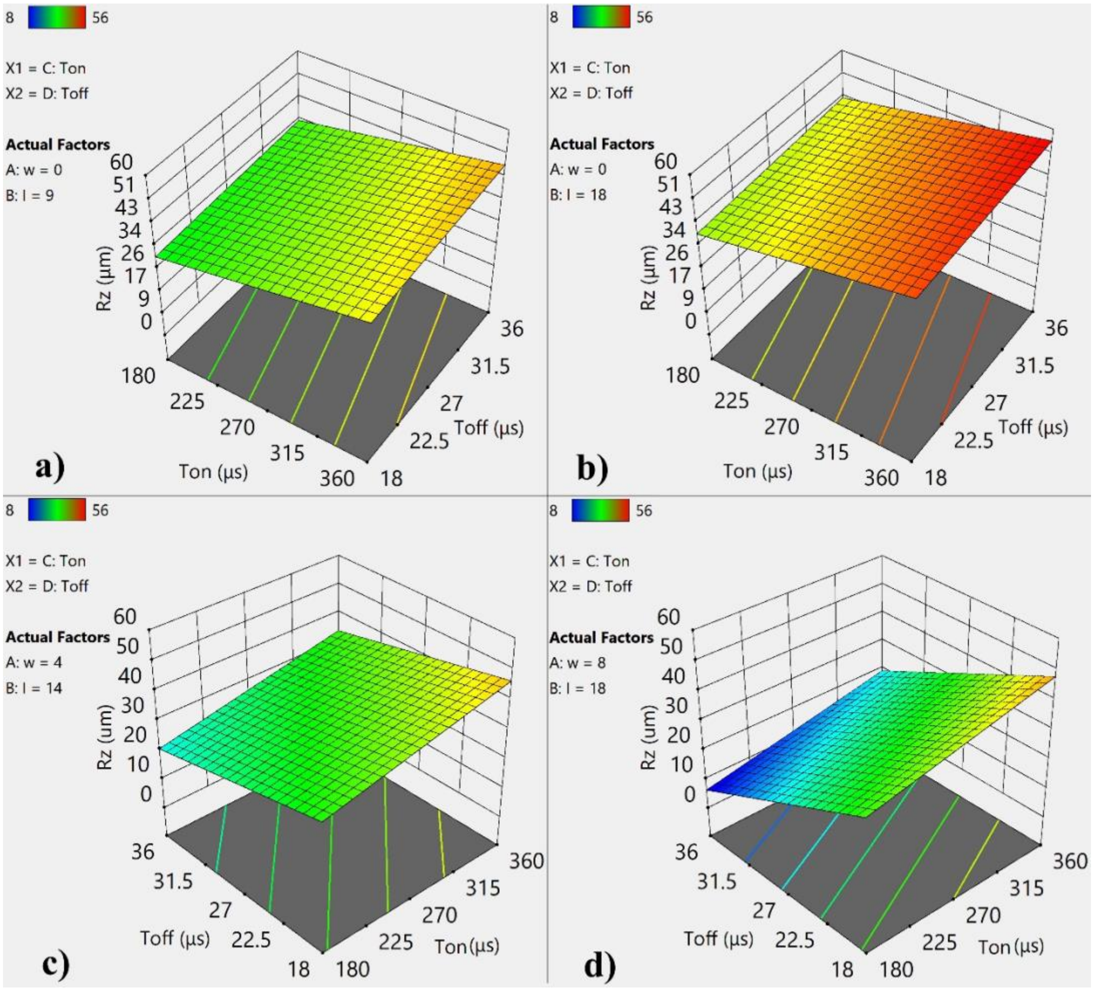

Figure 7. Change in R_z with T_{on} and T_{off} for constant values of a) w= 0, I= 9 A; b) w= 0, I= 18 A; c) w= 4 g/l, I=14 A; d) w= 8 g/l, I= 18 A

4. Conclusions and Recommendations

This study used RSM to model the effects of EDM parameters on R_a and R_z when processing a CoCr28Mo6 workpiece using an AISI 316L electrode with a Ti_6V_4Al dielectric liquid additive in various ratios. A Taguchi L_{16} experimental design was developed, and experimental PM-EDM processing was done using these design parameters to create regression models for R_a and R_z values.

The significance of developed R_a and R_z models are proven by p-values which are 0.0005 and 0.0003 respectively. In addition, R^2 values are 0.928 for the R_a model and 0.876 for the R_z model. It is concluded by these facts that these models can be utilized for the prediction of R_a and R_z values for varying powder concentration and machining conditions.

The following can be concluded from the response surface plots of the R_a and R_z models;

- R_a rises in response to a rise in powder concentration at the 180 µs level of T_{on}. However, as T_{on} increases to 360 µs, this scenario shifts, and R_a decreases as powder ratio falls.
- R_a is less affected by the powder ratio if the T_{off} value is raised. Similarly, the effect of T_{on} on R_a as the powder ratio increases.
- The effect of powder ratio on R_a varies in a complex way depending on the discharge current, T_{on}, and T_{off}.
- It is seen that increasing the current reduces the damping effect of T_{off} on R_a.
- R_a is more significantly impacted by T_{on} as the current levels rise.
- The R_z values rise for all values of the other components as the value of T_{on} increases.
- As T_{off} rises, the impact of the dust ratio on R_z grows.
- Increasing the current also increases the R_z values for all values of the other components.
- With an increase in powder ratio, T_{off} and T_{on} have a greater impact on R_z.
- Minimum value of R_a occurs with values of 8 g/l, 9 A, 360 µs, and 36 µs for powder ratio, discharge current, T_{on}, and T_{off} respectively.
- Minimum value of R_z occurs with values of 8 g/l, 18 A, 180 µs, and 36 µs for powder ratio, discharge current, T_{on}, and T_{off} respectively.

Acknowledgements

We would like to thank the Payas Vocational and Technical Anatolian High School Directorate for their support.

Authors' Contributions

All authors contributed equally to the study.

Statement of Conflicts of Interest

There is no conflict of interest between the authors.

Statement of Research and Publication Ethics

The author declares that this study complies with Research and Publication Ethics.

References

Abdel-Fattah, T. M., Loftis, D., & Mahapatro, A. (2011). Nanosized Controlled Surface Pretreatment of Biometallic Alloy 316L Stainless Steel. Journal of Biomedical Nanotechnology, 7(6), 794–800. https://doi.org/10.1166/jbn.2011.1346

Al-Amin, M., Abdul-Rani, A.-M., Aliyu, A. A., Bryant, M., Danish, M., & Ahmad, A. (2020). Bio-ceramic coatings adhesion and roughness of biomaterials through PM-EDM: a comprehensive review. Materials and Manufacturing Processes. https://doi.org/10.1080/10426914.2020.1772483

Ali, S., Rani, A. M. A., Mufti, R. A., Azam, F. I., Hastuty, S., Baig, Z., Hussain, M., & Shehzad, N. (2019). The Influence of Nitrogen Absorption on Microstructure, Properties and Cytotoxicity Assessment of 316L Stainless Steel Alloy Reinforced with Boron and Niobium. Processes.

Augustyn-Pieniążek, J., Lukaszczyk, A., & Zapala, R. (2013). Microstructure and Corrosion Resistance Characteristics of Cr-Co-Mo Alloys Designed for Prosthetic Materials. Archives of Metallurgy and Materials, 58(4), 1281–1285. https://doi.org/10.2478/amm-2013-0148

Cakir, M. v, Eyercioglu, O., Gov, K., Sahin, M., & Cakir, S. H. (2013). Comparison of Soft Computing Techniques for Modelling of the EDM Performance Parameters. Advances in Mechanical Engineering, 5, 392531. https://doi.org/10.1155/2013/392531

Chakmakchi, M., Ntasi, A., Mueller, W. D., & Zinelis, S. (2021). Effect of Cu and Ti electrodes on surface and electrochemical properties of Electro Discharge Machined (EDMed) structures made of Co-Cr and Ti dental alloys. Dental Materials, 37(4), 588–596. https://doi.org/https://doi.org/10.1016/j.dental.2021.01.012

David Whitehouse. (2002). Surfaces and Their Measurement. Hermes Penton Ltd.

Dinov, I. (2020). F distribution Tables. http://www.socr.ucla.edu/applets.dir/f_table.html

Elsiti, N. M., & Noordin, M. Y. (2017). Experimental Investigations into the Effect of Process Parameters and Nano-Powder (Fe2O3) on Material Removal Rate during Micro-EDM of Co-Cr-Mo. Key Engineering Materials, 740, 125–132. https://doi.org/10.4028/www.scientific.net/KEM.740.125

Elsiti, N., Mohd Yusof, N., & Idris, A. (2017). Effect of maghemite (γ-Fe2O3) nano-powder mixed dielectric medium on tool wear rate (TWR) during micro-EDM of CO-Cr-MO. Pertanika Journal of Science and Technology, 25, 847–858.

ERDEM, O., & KILIÇ, S. (2020). TiO2 Katkılı Çevre Dostu Dielektrik Sıvının Elektro Erozyon Delik Delme Performanslarının Araştırılması. Bilecik Şeyh Edebali Üniversitesi Fen Bilimleri Dergisi. https://doi.org/10.35193/bseufbd.713620

Fazira, M. F., Mohammad, M., Roslani, N., Saleh, M. H., & Ahmad, M. A. (2013). Low Strain Rate Upset Forging of Preformed CoCrMo Powder Alloy for Load Bearing Application: A Review. Procedia Engineering, 68, 405–410. https://doi.org/https://doi.org/10.1016/j.proeng.2013.12.199

Ho, K. H., & Newman, S. T. (2003). State of the art electrical discharge machining (EDM). International Journal of Machine Tools and Manufacture, 43(13), 1287–1300. https://doi.org/https://doi.org/10.1016/S0890-6955(03)00162-7

Iacono, F., Pirani, C., Generali, L., Sassatelli, P., Nucci, C., Gandolfi, M. G., & Prati, C. (2016). Wear analysis and cyclic fatigue resistance of electro discharge machined NiTi rotary instruments. Giornale Italiano Di Endodonzia, 30(1), 64–68. https://doi.org/https://doi.org/10.1016/j.gien.2016.04.006

Iranmanesh, S., Esmaeilzadeh, A., & Razavykia, A. (2017). Optimization of Electrical Discharge Machining Parameters of Co-Cr-Mo Using Central Composite Design. https://doi.org/10.1007/978-3-319-57078-5_5

Ho, K. H., & Newman, S. T. (2003). State of the art electrical discharge machining (EDM). International Journal of Machine Tools and Manufacture, 43(13), 1287–1300. https://doi.org/https://doi.org/10.1016/S0890-6955(03)00162-7

Jawahar, M., Sridhar Reddy, Ch., & Srinivas, Ch. (2019). A review of performance optimization and current research in PMEDM. Materials Today: Proceedings, 19, 742–747. https://doi.org/https://doi.org/10.1016/j.matpr.2019.08.122

Kumar, S. S., Erdemir, F., Varol, T., Kumaran, S. T., Uthayakumar, M., & Canakci, A. (2020). Investigation of WEDM process parameters of Al–SiC–B4C composites using response surface methodology. International Journal of Lightweight Materials and Manufacture, 3(2), 127–135. https://doi.org/https://doi.org/10.1016/j.ijlmm.2019.09.003

Mahajan, A., & Sidhu, S. S. (2019a). In vitro corrosion and hemocompatibility evaluation of electrical discharge treated cobalt–chromium implant. Journal of Materials Research, 34(8), 1363–1370. https://doi.org/10.1557/jmr.2019.73

Mahajan, A., & Sidhu, S. S. (2019b). Potential of electrical discharge treatment to enhance the in vitro cytocompatibility and tribological performance of Co–Cr implant. Journal of Materials Research, 34(16), 2837–2847. https://doi.org/DOI: 10.1557/jmr.2019.240

Mahajan, A., Sidhu, S. S., & Ablyaz, T. (2019). EDM Surface Treatment: An Enhanced Biocompatible Interface. In P. S. Bains, S. S. Sidhu, M. Bahraminasab, & C. Prakash (Eds.), Biomaterials in Orthopaedics and Bone Regeneration : Design and Synthesis (pp. 33–40). Springer Singapore. https://doi.org/10.1007/978-981-13-9977-0_3

Mahajan Amit and Sidhu, S. S. and A. T. (2019). EDM Surface Treatment: An Enhanced Biocompatible Interface. In S. S. and B. M. and P. C. Bains Preetkanwal Singh and Sidhu (Ed.), Biomaterials in Orthopaedics and Bone Regeneration : Design and Synthesis (pp. 33–40). Springer Singapore. https://doi.org/10.1007/978-981-13-9977-0_3

Mesalamy, A. S. El, & Youssef, A. (2020). Enhancement of cutting quality of abrasive waterjet by using multipass cutting strategy. Journal of Manufacturing Processes, 60, 530–543. https://doi.org/https://doi.org/10.1016/j.jmapro.2020.10.036

Myers, R. H., Montgomery, D. C., & Anderson-cook, C. M. (2016). Response Surface Methodology. In Wiley & Sons (Issue 4). https://doi.org/10.1007/s13398-014-0173-7.2

Ntasi, A., Mueller, W. D., Eliades, G., & Zinelis, S. (2010). The effect of Electro Discharge Machining (EDM) on the corrosion resistance of dental alloys. Dental Materials, 26(12), e237–e245. https://doi.org/10.1016/j.dental.2010.08.001

ÖPÖZ, T. T., YAŞAR, H, MURPHY, M. F, EKMEKCİ, N., and EKMEKCİ, B. (2019). Ti6Al4V Surface Modification by Hydroxyapatite Powder Mixed Electrical Discharge Machining for Medical Applications. International Journal of Advances in Engineering and Pure Sciences, 31, 1–10.

Prakash, C., Kansal, H. K., Pabla, B. S., & Puri, S. (2015). To optimize the surface roughness and microhardness of β-Ti alloy in PMEDM process using Non-dominated Sorting Genetic Algorithm-II. 2015 2nd International Conference on Recent Advances in Engineering & Computational Sciences (RAECS), 1–6. https://doi.org/10.1109/RAECS.2015.7453288

Rajkumar, H., & Vishwakamra, M. (2018). Performance Parameters Characteristics of PMEDM: A Review. In International Journal of Applied Engineering Research (Vol. 13, Issue 7). http://www.ripublication.com

Sales, W. F., Oliveira, A. R. F., & Raslan, A. A. (2016). Titanium perovskite (CaTiO3) formation in Ti6Al4V alloy using the electrical discharge machining process for biomedical applications. Surface and Coatings Technology, 307, 1011–1015. https://doi.org/10.1016/j.surfcoat.2016.10.028

Sharma, R., & Singh, J. (2014). Effect of Powder Mixed Electrical Discharge Machining (PMEDM) on Difficult-to-machine Materials – a Systematic Literature Review. 14(4), 233–255. https://doi.org/doi:10.1515/jmsp-2014-0016